

Controlled release of recombinant human cementum protein I from electrospun multiphasic scaffold for cementum regeneration

Xiaofeng Chen^{1,*}

Yu Liu^{1,*}

Leiyang Miao¹

Yangyang Wang²

Shuangshuang Ren¹

Xuebin Yang³

Yong Hu⁴

Weibin Sun¹

¹Department of Periodontology, Nanjing Stomatological Hospital, Medical School of Nanjing University, Nanjing, Jiangsu, People's Republic of China; ²Department of Materials Science and Engineering, College of Materials Science and Technology, Nanjing University of Aeronautics and Astronautics, Nanjing, Jiangsu, People's Republic of China; ³Biomaterials and Tissue Engineering Group, Leeds Dental Institute, University of Leeds, Leeds, UK; ⁴Institute of Materials Engineering, National Laboratory of Solid State Micro Structure, College of Engineering and Applied Sciences, Nanjing University, Nanjing, Jiangsu, People's Republic of China

*These authors contributed equally to this work

Correspondence: Weibin Sun
Department of Periodontology, Nanjing Stomatological Hospital, Medical School of Nanjing University, 30 Zhongyang Road, Xuanwu District, Nanjing, Jiangsu 210093, People's Republic of China
Tel +86 25 8362 0173
Fax +86 25 8362 0173
Email wbsun@nju.edu.cn

Abstract: Periodontitis is a major cause for tooth loss, which affects about 15% of the adult population. Cementum regeneration has been the crux of constructing the periodontal complex. Cementum protein 1 (CEMP1) is a cementum-specific protein that can induce cementogenic differentiation. In this study, poly(ethylene glycol) (PEG)-stabilized amorphous calcium phosphate (ACP) nanoparticles were prepared by wet-chemical method and then loaded with recombinant human CEMP1 (rhCEMP1) for controlled release. An electrospun multiphasic scaffold constituted of poly(ϵ -caprolactone) (PCL), type I collagen (COL), and rhCEMP1/ACP was fabricated. The effects of rhCEMP1/ACP/PCL/COL scaffold on the attachment proliferation, osteogenic, and cementogenic differentiations of human periodontal ligament cells, (PDLs) were systematically investigated. A critical size defect rat model was introduced to evaluate the effect of tissue regeneration of the scaffolds in vivo. The results showed that PEG-stabilized ACP nanoparticles formed a core-shell structure with sustained release of rhCEMP1 for up to 4 weeks. rhCEMP1/ACP/PCL/COL scaffold could suppress PDLs proliferation behavior and upregulate the expression of cementoblastic markers including CEMP1 and cementum attachment protein while downregulating osteoblastic markers including osteocalcin and osteopontin when it was cocultured with PDLs in vitro for 7 days. Histology analysis of cementum after being implanted with the scaffold in rats for 8 weeks showed that there was cementum-like tissue formation but little bone formation. These results indicated the potential of using electrospun multiphasic scaffolds for controlled release of rhCEMP1 for promoting cementum regeneration in reconstruction of the periodontal complex.

Keywords: nanofiber scaffold, rhCEMP1, controlled release, cementum regeneration, in vivo

Background

Periodontitis is a common oral inflammatory disease induced by periodontal pathogens that causes periodontal tissue destruction, including connective attachment loss and alveolar bone resorption, thereby resulting in tooth loss.¹ To date, periodontal reconstruction based on infection control is still the key solution for periodontal treatment. However, the bottle neck for periodontal reconstruction is that it is difficult to regenerate cementum. Cementum represents a unique avascular-mineralized connective tissue that covers the root surface of the teeth. It provides the interface through which Sharpey's collagen fibers of the periodontal ligament are anchored to the root surface. A number of studies show that cementum protein 1 (CEMP1, one kind of growth factor [GF]) promotes cell attachment, differentiation, extracellular matrix (ECM) deposition, and affects the composition, and morphology of hydroxyapatite (HA) crystals formed by human cementoblast cells in vitro.¹⁻⁵ These observations confirm that CEMP1 plays



an important role during the cementum formation and the biomineralization process.

However, there is lack of experimental data to ascertain the ability of recombinant human CEMP1 (rhCEMP1) to induce cementum regeneration *in vivo*. Although CEMP1 is beneficial for cementum regeneration, direct application of CEMP1 in tissue engineering is restricted due to its short biological half-life, systemic side effects, and rapid clearance. Given the obstacles surrounding the issue, we induced a sustained releasing system to fit with the tardy regeneration process of cementum.

Recently, biodegradable scaffolds have been designed and successfully used in the repair and regeneration of damaged or diseased tissues. In addition, GFs can be encapsulated within these scaffolds to circumvent the premature release and the degradation of the GF before it reaches the targeting site. GFs encapsulated inside these scaffolds can be released according to cellular demands in a controlled manner,⁶ allowing similar reparative processes to be induced by low GF concentration.⁷ Importantly, controlled release of vascular endothelial growth factor from the scaffold leads to the formation of a more organized vasculature in comparison to the vasculature that arises from the uncontrolled vascular endothelial growth factor release.⁸ Furthermore, multiple GFs can be incorporated in one scaffold, which may complement one another temporally and spatially.^{9,10} However, scaffolds fabricated with a sole component usually exhibit limited mechanical properties and fail to mimic the natural tissue. To address this shortcoming, biomimetic hybrid scaffolds composed of polymer and calcium phosphate nanoparticles were developed to successfully regenerate human tooth–ligament interfaces.¹¹ The calcium phosphate not only enhanced the toughness of the scaffold, but also improved its biocompatibility and accelerated the biomineralization procedure, because the chemical composition of calcium phosphate is similar to the inorganic phase of bone. Therefore, CEMP1-encapsulated scaffolds seem to be suitable in the cementum formation and the biomineralization process, which not only acts as a physical and biological support for cementum regeneration, but also a three-dimensional (3D) artificial cementum ECM to mimic the structure and function of cementum.

Inspired by the merits of the hybrid scaffold, in this work, a robust CEMP1-encapsulated hybrid scaffold composed of poly(ϵ -caprolactone) (PCL), Type I collagen (COL), and poly(ethylene glycol) (PEG)-modified amorphous calcium phosphate (ACP) [$\text{Ca}_3(\text{PO}_4)_2 \cdot 3\text{H}_2\text{O}$] was designed and fabricated through electrospinning method. PCL possesses remarkable toughness and good biocompatibility in addition to a high elongation and fracture energy.^{12–14} Its flexibility

has been used to overcome the brittleness and low elongation property of pure inorganic scaffolds.¹⁵ COL and calcium phosphate are the main constituents of cementum ECM.¹⁶ The presence of COL in the scaffold is conducive to tissue regeneration, including good biocompatibility, no immunogenicity, no toxicity, and supporting, protecting, and mediating cell adhesion.¹⁷ The use of ACP has some advantages: ACP shows better osteoconductive property than HA *in vivo* and its biodegradability is higher than that of tricalcium phosphate.¹⁸ Furthermore, the conversion of ACP to HA will release functional calcium and phosphate ions as convenient and fast sources of raw materials for the regeneration of mineralized tissue.¹⁹

To maintain the bioactivity of CEMP1 during the electrospinning, rhCEMP1 was first encapsulated inside PEG-modified ACP, due to the tight affinity between CEMP1 and calcium phosphate.²⁰ The encapsulation of rhCEMP1 inside the PEG-modified ACP can protect rhCEMP1 from contacting the organic solvent during the electrospinning, thus avoiding unwanted protein denaturation. The release of rhCEMP1 from the rhCEMP1/ACP nanoparticles was studied. Then an electrospun multiphase scaffold composed of rhCEMP1/ACP, PCL, and COL was fabricated and cocultured with periodontal ligament cells (PDLCs) to assess the biocompatibility and inductivity. Finally, the *in vivo* assessment of tissue regeneration was conducted in a critical size defect rat model.

Materials and methods

Materials and reagents

All reagents and chemicals were purchased from Aladdin (Shanghai, People's Republic of China) unless otherwise stated. Plasmids and BL21 (DE3) were purchased from Thermo Fisher Scientific (Waltham, MA, USA). rhCEMP1 enzyme-linked immunosorbent assay kit was purchased from CUSABIO (Wuhan, Hubei, People's Republic of China). PCL was purchased from Dai Gang Biology (PCL, molecular weight of 160 kDa; Shanghai, People's Republic of China). COL was purchased from Sigma-Aldrich (Wadena, MN, USA) and α -minimum essential medium (α -MEM) was from Hyclone (Logan, UT, USA). Fetal bovine serum and antibiotics were purchased from Gibco (Grand Island, NY, USA).

Synthesis and characterization of ACPs and rhCEMP1-loaded ACPs (ACPPs) nanoparticles

Briefly, CaCl_2 and PEG (molecular weight: 10,000) with designed ratios of 1:1 (w/w) were dissolved in distilled water to form 0.1 M solution of CaCl_2 , which was immersed in an ice-water bath. Then $\text{Na}_3\text{PO}_4 \cdot 12\text{H}_2\text{O}$ aqueous solution

(0.133 M) was added into the CaCl₂/PEG solution with a Ca/P mole ratio of 1.5, and the reaction was continued in ice water under 900 rpm stirring for 30 minutes. The ACP nanoparticles were obtained by washing the precipitates with distilled water repeatedly to remove the unwanted ions (Na⁺ and Cl⁻) and freeze-dried for 48 hours. The blank calcium phosphate samples were prepared without the presence of PEG, as the control.

For the preparation of ACPPs, 5 mL distilled water was added to suspend the ACP precipitates. A specified amount of lyophilized rhCEMP1 (as listed in Table 1) powder was allowed to incorporate into the ACP precipitates by stirring at 900 rpm for 5 minutes in an ice-water bath to afford a mixture in which the net share of rhCEMP1 in dry state would be 1%, 2%, 5%, and 8% (w/w). The new precipitates containing rhCEMP1 were named ACPPs and freeze-dried for 48 hours.

Production of rhCEMP1 has been described in earlier studies.²¹ Briefly, rhCEMP1 complementary DNA (cDNA) was optimized and inserted into corresponding sites of intermediate vector pENTR/SD/D after restriction endonuclease digestion, and then inserted into vector pET28a. The recombinant vector pET28a-rhCEMP1 was confirmed by agarose gel electrophoresis and DNA sequence analysis. The plasmid was introduced into BL21 (DE3) expression host *Escherichia coli* strain. The expression of rhCEMP1 was determined by sodium dodecyl sulfate–polyacrylamide gel electrophoresis and enzyme-linked immunosorbent assay.

The precipitates obtained in the absence and presence of PEG or rhCEMP1 were characterized by transmission electron microscopy (JEM-200CX; JEOL, Tokyo, Japan). Fourier-transform infrared spectroscopy (NEXUS870; NICOLET, San Carlos, CA, USA) was conducted in the range of 400–4,000 cm⁻¹.

Encapsulation efficiency and controlled release of rhCEMP1 from ACPPs

About 10 mg of the freeze-dried ACPPs were dispersed in 10 mL of phosphate-buffered saline (PBS) in a shaker incubator at 100 rpm and 37°C for 5 minutes. Afterwards, the solution was centrifuged and the concentration of rhCEMP1 in the supernatant was assessed using rhCEMP1

enzyme-linked immunosorbent assay kit. The ratio of supernatant to actual protein weight was defined as encapsulation efficiency (EE) of the nanoparticles. The EE of rhCEMP1 was calculated as:

$$EE (\%) = \frac{C_t - C_f}{C_t} \times 100, \quad (1)$$

where C_f is the weight of free rhCEMP1 in the supernatant and C_t is the actual protein weight.

About 10 mg ACPPs were immersed into 10 mL of PBS (pH 7.4), and the samples were placed in a shaker incubator at 100 rpm and 37°C. At predetermined intervals (1, 3, 7, 14, 21, and 28 days), the medium was retrieved and an equal volume of fresh medium was replenished. The amounts of rhCEMP1 in the release medium were ascertained by rhCEMP1 enzyme-linked immunosorbent assay kit.

Fabrication of electrospun multiphasic scaffold

Two kinds of scaffold were prepared using the electrospinning technique and named as ACP/COL/PCL and ACP/rhCEMP1/COL/PCL. A solution strategy was adopted in polymer blending, and the detailed compositions are listed in Table 2. COL and PCL (weight ratio =1/1) were dissolved in hexafluoroisopropanol to yield a 25 w/v% solution. ACP or rhCEMP/ACP-containing scaffolds were generated by admixing ACP or rhCEMP/ACP (a dispersion of 20 w/v% in hexafluoroisopropanol) to the polymer blend solutions (ACPP1 was chosen for fabricating the scaffold and then named as rhCEMP/ACP afterwards). A defined amount of genipin (GP) was added to cross-link the collagen before electrospinning. GP is a natural cross-linking agent extracted from the gardenia plant, and is less cytotoxic than glutaraldehyde. GP can react with proteins and produce blue-colored fluorescent hydrogels, thereby enabling cross-linking.²² The solution was drawn into a 10 mL syringe attached with a tip-blunt capillary (inner diameter =0.34 mm). A needlelike flow of the solution from the capillary spinneret was fed by a syringe pump at a flow rate of 2.5 mL/h. A high-voltage power supply was used at 17 kV. The distance between the tip-blunt capillary and the

Table 1 The compositions of electrospinning solutions

Sample	HFIP (mL)	COL (mg)	PCL (mg)	ACP (mg)	ACP/rhCEMP1 (mg)	GP (mg)
ACP/COL/PCL	10	900	900	600	0	12
ACP/rhCEMP1/COL/PCL	10	900	900	0	600	12

Abbreviations: ACP, amorphous calcium phosphate; COL, Type I collagen; GP, genipin; HFIP, hexafluoroisopropanol; PCL, poly(ϵ -caprolactone); rhCEMP1, recombinant human cementum protein 1.

Table 2 The compositions of ACPs

Sample	CaCl ₂ (mg)	Na ₃ PO ₄ ·12H ₂ O (mg)	PEG (mg)	diH ₂ O-A (mL)	diH ₂ O-B (mL)	rhCEMPI (mg)
ACP	367.5	842.6	0	50	0	0
ACPP0	367.5	842.6	367.5	50	0	0
ACPP1	367.5	842.6	367.5	50	5	3.4
ACPP2	367.5	842.6	367.5	50	5	6.8
ACPP5	367.5	842.6	367.5	50	5	17.0
ACPP8	367.5	842.6	367.5	50	5	27.2

Abbreviations: ACP, amorphous calcium phosphate; PEG, poly (ethylene glycol); ACPP1, 1% (w/w) rhCEMPI in ACP/PEG; ACPP2, 2% (w/w) rhCEMPI in ACP/PEG; ACPP5, 5% (w/w) rhCEMPI in ACP/PEG; ACPP8, 8% (w/w) rhCEMPI in ACP/PEG; di, deionized; rhCEMPI, recombinant human cementum protein I.

cover slips or aluminum foil that were used as collectors was 15 cm. The obtained electrospun fibers were dried and then stored in clean polythene bags for further use.²³

Culture and seeding of PDLCs

Human PDLCs were retrieved, using a method adopted from Tanaka et al,²⁴ from sound premolars extracted for orthodontic reasons from five individuals (16–18 years old, three males and two females). All procedures in the study in both in vitro cell culture and in vivo animal model followed the approved ethical guidelines set by the Ethics Committee of Nanjing Stomatological Hospital. Written informed consent was obtained from all five individuals and/or their parents/guardians. Briefly, teeth were rinsed three times with PBS supplemented with antibiotics (streptomycin 100 µg/mL, penicillin 100 units/mL). Periodontal ligament tissue was scraped from the middle-third of root surface with a surgical scalpel and cultured in α-MEM supplemented with 10% fetal bovine serum and antibiotics (streptomycin 100 mg/mL, penicillin 100 units/mL) in an atmosphere of 95% air/5% CO₂ at 37°C with 100% humidity. Cells were cultured in vitro and the third passage was used for the experiments.

The scaffolds were cut into circular discs with diameters of 5 mm (for 96-well plate), 19 mm (for 12-well plate), and 25 mm (for 6-well plate) and sterilized in 70% ethanol for 40 minutes and then washed with the culture medium to remove the alcohol residue. The cells were seeded on the sterilized scaffolds with a density of 6×10³ cells/cm² and were incubated at 37°C for 4 hours to promote cell attachment/adhesion. Then, 1 mL of culture medium was added into each well. The culture medium was changed every 2 days.

Assessment of PDLCs attachment, proliferation, and viability on 3D scaffolds

The cell viability and proliferation on the scaffolds was assessed using 3-(4,5-dimethylthiazol-2-yl)-2,5-diphenyltetrazolium bromide (MTT) assay. At predetermined time intervals (1, 3, and 7 days), the scaffolds were washed with PBS to

remove nonadherent cells, and 10% MTT solution in α-MEM was added, followed by incubation for 3 hours; afterwards, the formazan crystals were dissolved in dimethyl sulfoxide. The absorbance of the solutions at 490 nm was recorded.

Morphology of the cells on the scaffolds was observed by scanning electron microscopy (SEM). At day 1, 3, and 7, the cell-seeded scaffolds were washed with PBS and fixed in 2.5% glutaraldehyde, followed by dehydration in incremental concentrations of ethanol (15%, 30%, 50%, 70%, 80%, 90%, and 100%) for 10 minutes each. Then, the specimens were dried at room temperature and coated with gold to be observed using SEM (S-3400N II; Hitachi, Tokyo, Japan).

Effect of multiphasic scaffolds on osteogenic and cementogenic differentiation of PDLCs

To investigate the effect of multiphasic scaffold on the osteogenic-related gene expression of osteocalcin (*OCN*), osteopontin (*OPN*), cementogenic-related gene expression of *CEMPI*, and cementum attachment protein (*CAP*), PDLCs were seeded on ACP/PCL/COL or rhCEMPI/ACP/PCL/COL scaffolds (PDLCs without scaffold were used as the control) and cultured in osteogenic differentiation medium 10% FBS α-MEM (Sigma-Aldrich) in the presence of osteogenic supplements, namely, ascorbic acid (50 µg/mL; Biosharp, Carlsbad, CA, USA), β-glycerolphosphate (10 mM; Biosharp), and dexamethasone (10⁻⁸ M; Biosharp) for up to 7 days. Total RNA was isolated from the cultured scaffolds using RNAiso plus (Takara, Tokyo, Japan). RNA concentration and purity were determined using a Nanodrop ND 1000 Spectrophotometer (NanoDrop Technologies, Wilmington, DE, USA). Total RNA was prepared from cells using the RNaseasy Mini Kit according to the manufacturer instructions (Qiagen, Venlo, the Netherlands). One microgram of total RNA was used for cDNA synthesis using a PrimeScript™ II 1st Strand cDNA Synthesis Kit for real-time polymerase chain reaction (RT-PCR; Takara). Quantitative RT-PCR was carried out using Universal SYBR Green Supermix (Bio-Rad,

Hercules, CA, USA). Primer sequences are listed in Table 3. Amplification conditions were 95°C for 10 minutes for denaturation, then 40 cycles of 95°C for 15 seconds, 60°C for 1 minute, and 95°C for 15 seconds, followed by a melting curve from 58°C to 98°C. Reaction products were quantified using StepOne Software (Version 2.1). Expression level values were normalized to that of an internal control, β -actin.

Implantation in rat calvaria model

The rat calvarial defect is generally used to evaluate bone regeneration in an orthotopic model and to screen biomaterials or tissue engineering constructs before moving to larger animals for potential translation to human applications. All procedures followed the approved ethical guidelines set by the Ethics Committee of Nanjing Stomatological Hospital. This size of defect was chosen because it is the “critical size”: a defect of this size does not heal by itself without intervention.²⁵

Rats with calvarial defects were divided into three groups, ACP/COL/PCL, rhCEMPI/ACP/COL/PCL, and control, with each group having six rats. To achieve this, 27 male Wistar rats aged 7–8 weeks weighing 240–290 g were obtained from Model Animal Research Center of Nanjing University. The rats were positioned in a stereotaxic frame and immobilized during surgery. The hair over the skull of the animals was shaved, a full-thickness skin incision was made along the midline from the nasofrontal to occipital region, then the subcutaneous tissue was dissected, and the underlying periosteum was sharply incised/elevated to obtain sufficient exposure to the calvarium. A saline-cooled stainless steel trephine (5 mm outer diameter) was used to remove a full-thickness of bone to create the critical bone defects on both left and right sides of dorsal calvarium. Substantial caution was taken to prevent damage to the underlying sagittal sinus and dura mater. Then the bone defects were

repaired with a 5 mm diameter scaffold of either ACP/PCL/COL or rhCEMPI/ACP/PCL/COL. In the control group, the defect was left empty without repair. The periosteum and the subcutaneous tissue were closed sequentially with absorbable sutures. The skin wound was closed with 4–0 silk sutures. The animals were kept on a surgical bed until they awoke and had free access to food and water thereafter.

After 4 and 8 weeks postimplantation, the animals were sacrificed by CO₂ asphyxiation and the calvaria bone of the rat was harvested and fixed in 10% formalin for 48 hours. The fixed samples were washed with PBS and were processed and analyzed histologically and by micro-computed tomography (CT).

Micro-CT

Micro-CT of all specimens was performed using an X-eye micro-CT scanner (SEC, Gyeonggi-do, Korea) that has a very high spatial resolution through 360° and is equipped with an X-ray charge-coupled device camera of 1.4 M. The maximum tube current was 0.2 mA, maximum tube voltage was 160 kV, and the focus size was 1 μ m. For each sample, 70 V tube voltage and 70 A current were maintained in the X-ray tube. To scan the whole calvaria, 400 microtomographic slices of every sample were taken with a slice increment of 30 μ m. The micro-CT slices were processed using 3Di-Cat thresholding, then used to create 3D models for visualization and quantitative histomorphometric analysis.

Histological staining

After fixation in 10% neutral buffered formalin, the samples were rinsed with PBS several times and decalcified in 0.5% formaldehyde containing 10% ethylene diamine tetraacetic acid, pH 7.4, at 37°C in an incubator shaker. Then, the samples were embedded in tissue embedder (KMA-0100-00; CellPath Ltd., Newtown, UK), and 5 μ m thick sections were prepared. Sections were perpendicular to the sagittal suture to produce a plane of analysis through the center of the defect. Representative sections were stained with H&E (hematoxylin and eosin). Additionally, Masson’s trichrome was visualized using an optical microscope for cross-reference.

Statistical analysis

All the experiments were repeated three times, with each treatment conducted in triplicate unless otherwise stated. Data are represented as averages \pm standard deviation and analyzed statistically by one-way analysis of variance (ANOVA) and a post hoc Student’s *t*-test. The post hoc *t*-test was performed when the ANOVA test indicated significance at $P < 0.05$.

Table 3 Primer pairs used in qRT-PCR analysis

Gene	Primers
OCN	F: 5'-CACTCCTCGCCCTATTGGC-3' R: 5'-CCCTCCTGCTTGGACACAAAG-3'
OPN	F: 5'-CTCCATTGACTCGAACGACTC-3' R: 5'-CAGGTCTGCGAAACTTCTTAGAT-3'
CAP	F: 5'-TCCAGACATTTGCCTTGCTT-3' R: 5'-TTACAGCAATAGAAAAACAGCATGA-3'
CEMPI	F: 5'-GGCGATGCTCAACCTTAAC-3' R: 5'-GATACCCACCTCTGCCTTGA-3'
β -actin	F: 5'-GATGAGATTGGCATGGCTTT-3' R: 5'-CACCTTACCCTTCCAGTTT-3'

Abbreviations: CAP, cementum attachment protein; *CEMPI*, cementum protein 1; OCN, osteocalcin; OPN, osteopontin; qRT-PCR, quantitative real-time polymerase chain reaction; F, forward primer; R, reverse primer.

Results

Characterization of ACPs

ACP nanoparticles obtained without the presence of PEG have a needlelike shape as shown in Figure 1A, which suggests the transformation of ACP to apatite because of the quick hydrolysis of ACP during the initial synthesis procedure.²¹ After the addition of PEG, the as-prepared ACP nanoparticles were covered by PEG, which hampered their hydrolysis. Consequently, a core-shell structure was clearly observed in Figure 1B. The gray shell is the PEG layer and the core is made of ACP (Figure 1B inset). After the incorporation of rhCEMP1 into the ACP nanoparticles, irregular morphology was observed, confirming the successful encapsulation of rhCEMP1 (Figure 1C).

Infrared spectroscopy was conducted to measure the chemical composition of these samples. Figure 2 shows the spectra of rhCEMP1, ACP, ACP/PEG, rhCEMP1/ACP/PEG, and their characteristic peaks. The characteristic vibration peaks of tetrahedral PO_4^{3-} ions at 590–610 cm^{-1} and around 1,000 cm^{-1} are clearly observed in the infrared spectrum of ACP (Figure 2).²⁶ The large and strong bands at 2,886 cm^{-1} were attributed to CH_2 stretch in the spectrum of ACP/PEG, and the shoulder at 842 cm^{-1} was attributed to C–O stretch,²⁷ confirming the presence of PEG. The characteristic peaks of amide I and amide II of rhCEMP1 at 1,653 and 1,547 cm^{-1} ,²⁸ as well as the bending vibration of PEG near 842 cm^{-1} were all observed in rhCEMP1/ACP/PEG. These results further confirmed the encapsulation of rhCEMP1 inside the ACPs.

EE and controlled release of rhCEMP1 from ACPs

The loading ratios and EEs were measured, and the results are shown in Figure 3A. When these ACP/PEG nanoparticles were immersed in the rhCEMP1 solution at different concentrations (1%, 2%, 5%, and 8% [w/w]), the EE

of rhCEMP1 inside ACP/PEG was 97.8 ± 2.2 , 96.4 ± 1.2 , 81.3 ± 3.6 , and 81.3 ± 3.6 , respectively.

Cumulative release profiles of rhCEMP1 from the rhCEMP1/ACP/PEG are presented in Figure 3B. In the case of ACP1 and ACP2, containing low content of rhCEMP1, an ultimately low burst release on the first day ($1.72\% \pm 0.07\%$ for ACP1 and $1.86\% \pm 0.46\%$ for ACP2) was observed, followed by the continuously sustained release up to 4 weeks. For the ACP5 and ACP8, the initial burst release on day 1 was $10.1\% \pm 1.5\%$ and $20.4\% \pm 2.4\%$, respectively. These results indicated that these ACP/PEG nanoparticles could load rhCEMP1 well and release it in a sustained manner.

Characterization of electrospun multiphasic scaffold

The meshes of electrospun nanofibers showed a porous morphology as they were observed in the SEM images (Figure 4). The average diameter of PCL/COL, ACP/PCL/COL, and rhCEMP1/ACP/PCL/COL fibers was determined to be 130, 214, and 204 nm, respectively. Electrospun fibers loaded with ACPs demonstrated a rough surface with protuberances (Figure 4D and E). Energy dispersive X-ray spectroscopy was used for the elemental analysis of the scaffolds. In contrast with PCL/COL, the calcium and phosphorus elements were observed both in the ACP/PCL/COL and rhCEMP1/ACP/PCL/COL scaffolds, further indicating the presence of ACP in the scaffolds (Figure 4F and I).

The proliferation of PDLCs on the scaffolds

At day 1, 3, and 7 after cell seeding, SEM showed that PDLCs could attach and grow on the multiphasic scaffolds ACP/PCL/COL (Figure 5A–C). The cells adhering to the fibers appeared to have rounded or spindle-shaped morphology. From Figure 5D–F, it can be seen that the PDLCs can not only attach but also spread on the surface of the scaffold.

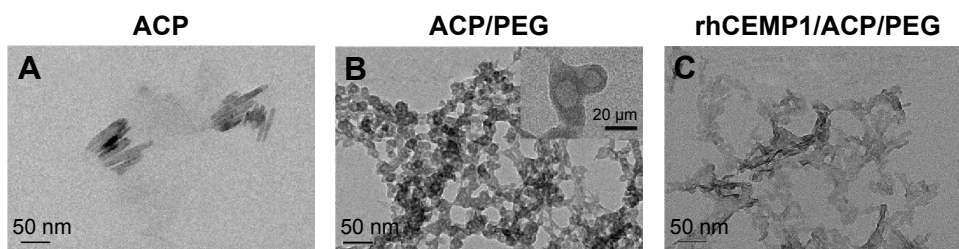


Figure 1 Transmission electron micrographs of ACPs prepared with or without PEG and rhCEMP1.

Notes: (A) ACP nanoparticles obtained without the presence of PEG had a needlelike shape. (B) The addition of PEG in ACP resulted in a core-shell structure. (C) After the incorporation of rhCEMP1 into the ACP nanoparticles, irregular morphology was observed.

Abbreviations: ACP, amorphous calcium phosphate; PEG, poly(ethylene glycol); rhCEMP1, recombinant human cementum protein I.

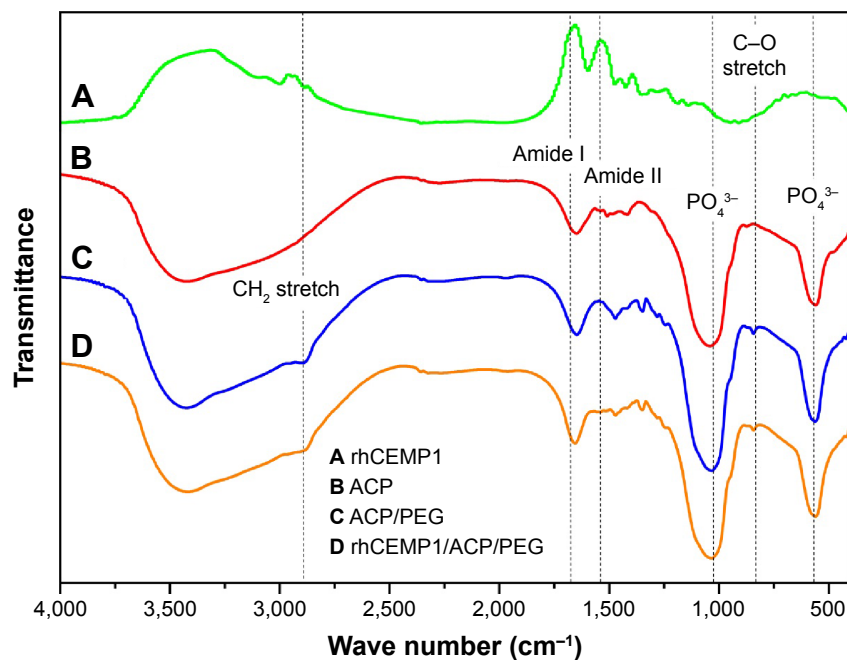


Figure 2 FTIR spectra of ACPs.

Notes: (A) rhCEMP1, (B) ACP, (C) ACP/PEG, and (D) rhCEMP1/ACP/PEG. The characteristic vibration peaks of tetrahedral PO_4^{3-} ions at 590–610 cm^{-1} and around 1,000 cm^{-1} are clearly observed in the FTIR spectrum of ACP. The large and strong bands at 2,886 cm^{-1} are attributed to CH_2 stretch and the shoulder at 842 cm^{-1} are attributed to C–O stretch, confirming the presence of PEG. The characteristic peaks of amide I and amide II of rhCEMP1 are at 1,653 and 1,547 cm^{-1} .

Abbreviations: ACP, amorphous calcium phosphate; FTIR, Fourier-transform infrared spectroscopy; PEG, poly(ethylene glycol); rhCEMP1, recombinant human cementum protein I.

Cells on rhCEMP1/ACP/PCL/COL exhibited extended distended, spread morphology. The PDLCs proliferated stably during a prolonged culture period on/within ACP/PCL/COL scaffold, but rhCEMP1/ACP/PCL/COL tended to suppress the growth of cells (Figure 5G).

Effect of rhCEMP1/ACP/PCL/COL scaffold on cementogenic and/or osteogenic differentiation of PDLCs in vitro

The scaffolds were cocultured with PDLCs for 7 days. To determine if scaffolds induce osteogenic and/or cementogenic

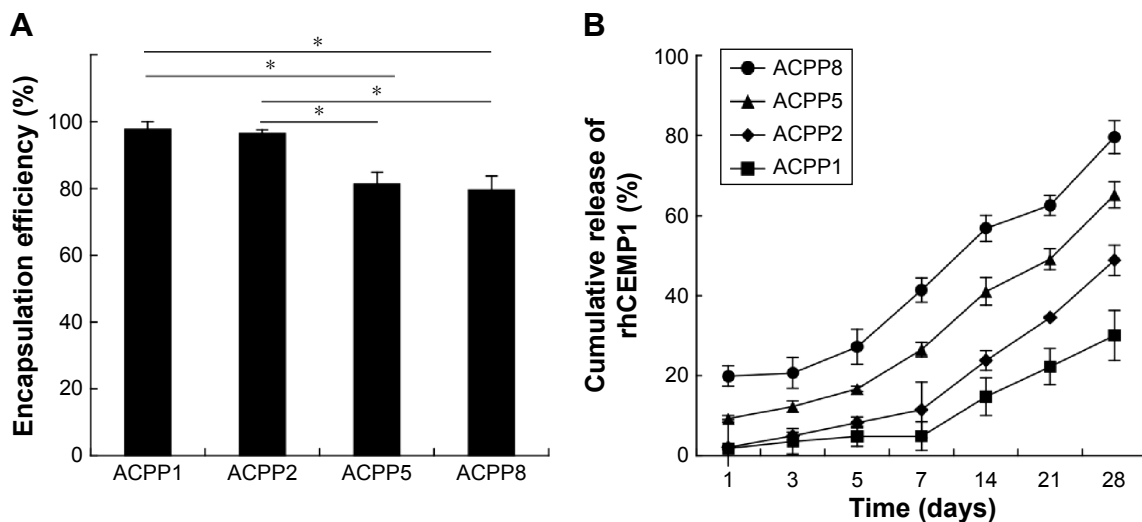


Figure 3 rhCEMP1 EE and release profile.

Notes: (A) The EE was correlated reciprocally with the concentration of rhCEMP1 inside ACP/PEG. (B) Cumulative release profiles of rhCEMP1 from the rhCEMP1/ACP/PEG went through a low burst release on the first day, followed by the continuously sustained release up to 4 weeks. The results are presented as means \pm standard deviation ($n=3$); * $P<0.05$.

Abbreviations: ACP, amorphous calcium phosphate; ACPP1, 1% (w/w) rhCEMP1 in ACP/PEG; ACPP2, 2% (w/w) rhCEMP1 in ACP/PEG; ACPP5, 5% (w/w) rhCEMP1 in ACP/PEG; ACPP8, 8% (w/w) rhCEMP1 in ACP/PEG; EE, encapsulation efficiency; PEG, poly(ethylene glycol); rhCEMP1, recombinant human cementum protein I.

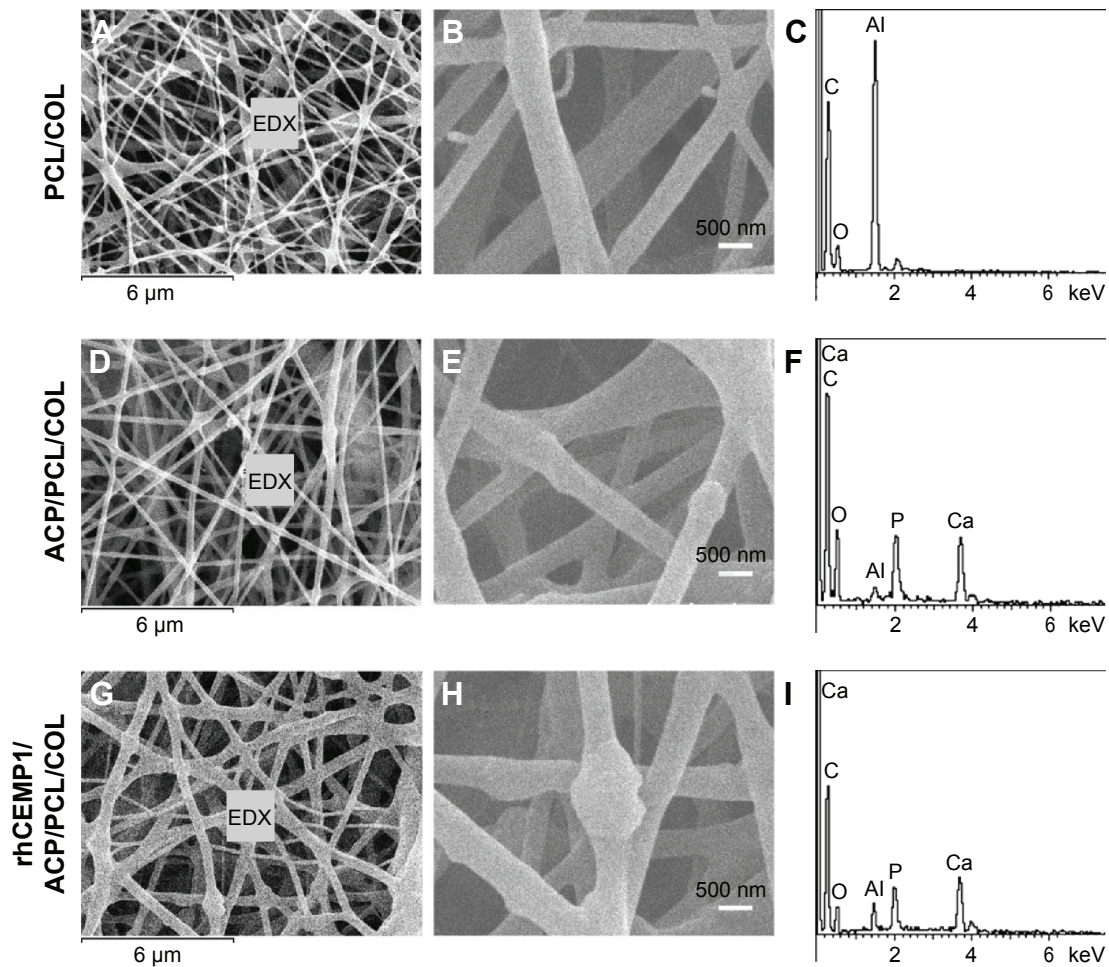


Figure 4 The morphology and elemental composition of scaffolds. **Notes:** (A) SEM image of PCL/COL with interconnected pores; (B) higher magnification SEM image exhibited smooth surface; (C) EDX results suggested no Ca and P present; (D) ACP/PCL/COL with a rough surface and a diameter of about 200 nm; (E) higher magnification SEM image shows the surface roughness of the fibers; (F) the peaks of Ca and P suggested the presence of ACP. (G) rhCEMP1/ACP/PCL/COL scaffolds with (H) higher magnification SEM image to show the surface roughness of the fibers; and (I) the peaks of Ca and P suggested the presence of rhCEMP1/ACP. **Abbreviations:** ACP, amorphous calcium phosphate; COL, type I collagen; EDX, energy-dispersive X-ray spectroscopy; PCL, poly(ϵ -caprolactone); rhCEMP1, recombinant human cementum protein I; SEM, scanning electron microscopy.

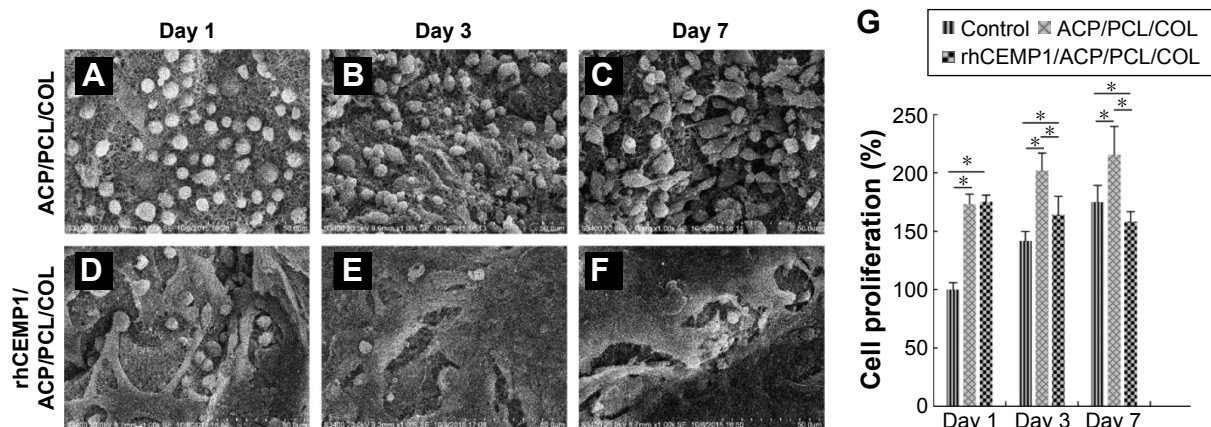


Figure 5 Morphology of PDLCs on scaffolds. **Notes:** At days 1, 3, and 7 after cell seeding, SEM showed the PDLCs could attach and grow on the multiphase scaffolds ACP/PCL/COL. The cells adhering to the fibers appeared as rounded or spindle-shaped morphology (A–C). Cells on rhCEMP1/ACP/PCL/COL exhibited extended distended, spread morphology (D–F). The PDLCs proliferated stably during a prolonged culture period on/within ACP/PCL/COL scaffold, but rhCEMP1/ACP/PCL/COL tended to suppress the growth of cells (G). SEM images were taken at 1,000 \times magnification; * $P < 0.05$. **Abbreviations:** ACP, amorphous calcium phosphate; COL, Type I collagen; PCL, poly(ϵ -caprolactone); PDLCs, periodontal ligament cell; rhCEMP1, recombinant human cementum protein I; SEM, scanning electron microscopy.

differentiation, the expressions of cementogenic markers (*CAP* and *CEMP1*) and osteogenic gene markers (osteocalcin – *OCN* and osteopontin – *OPN*) were analyzed by quantitative PCR (Figure 6). ACP/PCL/COL upregulated the expression of *CAP* and *CEMP1* (up to 2- and 20-fold). Moreover, it increased *OCN* and *OPN* expression significantly by 16- and 3-fold, respectively. This indicated that ACP/PCL/COL facilitated both osteogenesis and cementogenesis. The ability of cementogenesis was intensified for

rhCEMP1/ACP/PCL/COL compared to ACP/PCL/COL, with 44-fold *CAP* and 5-fold *CEMP1* expression. In contrast, the expression of *OCN* was rather limited with rhCEMP1/ACP/PCL/COL and it was just one-fifth of ACP/PCL/COL. Notably, the expression of *OPN* could not be detected. This result proved that rhCEMP1/ACP/PCL/COL had the ability to induce cementogenic differentiation of PDLCs. Meanwhile, it controlled osteogenesis; therefore, there would be more chances for cementogenesis.

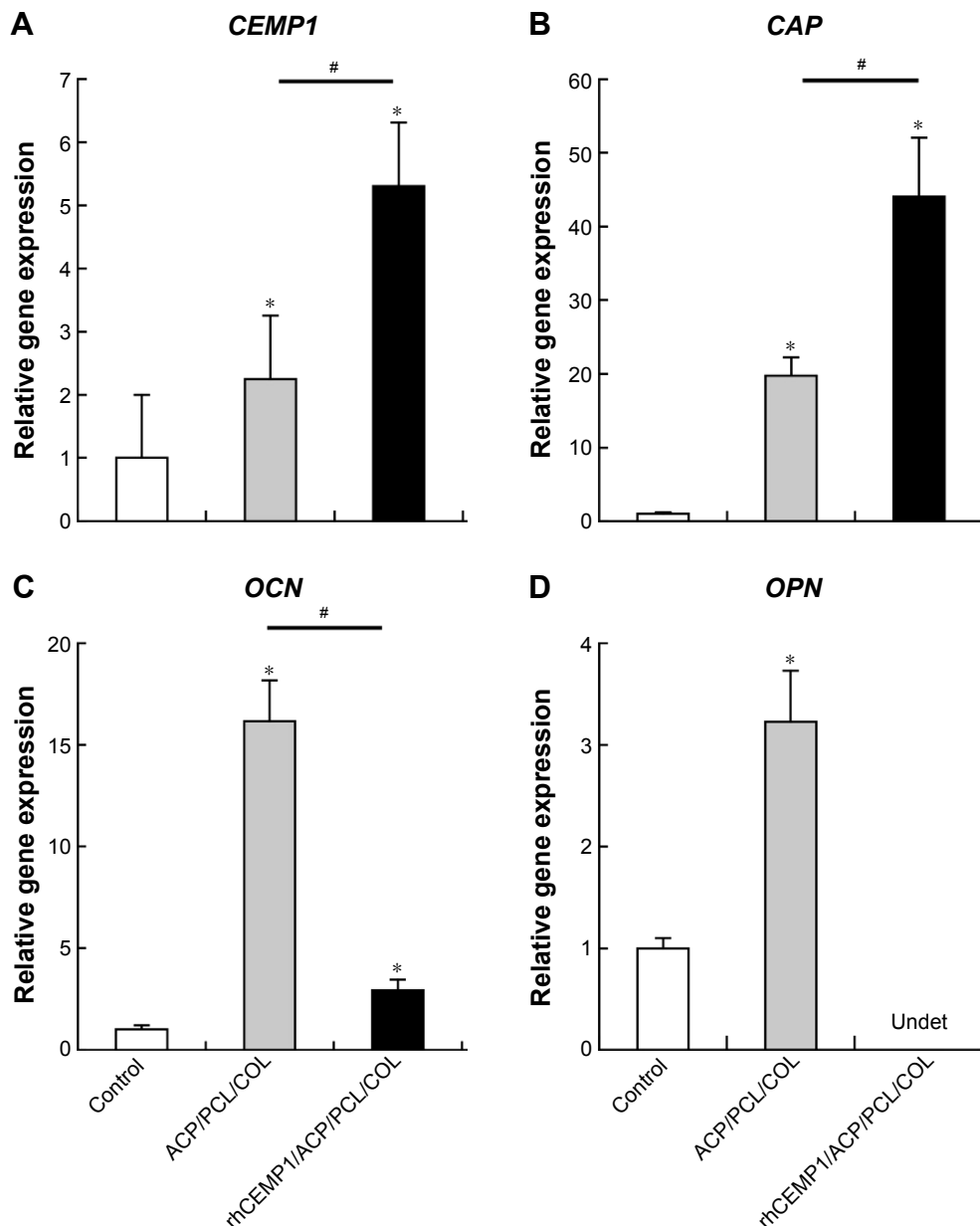


Figure 6 Gene expression by PDLCs seeded on the scaffolds at day 7 of culture.

Notes: ACP/PCL/COL upregulated the expression of *CAP* (A) and *CEMP1* (B). The ability of cementogenesis was intensified for rhCEMP1/ACP/PCL/COL compared to ACP/PCL/COL. ACP/PCL/COL increased *OCN* and *OPN* expression. In contrast, the expression of *OCN* was rather limited with rhCEMP1/ACP/PCL/COL (C). Notably, the expression of *OPN* could not be detected (D). Data are mean \pm SD (n=3) normalized to β -actin, then relative to control. * $P < 0.05$ versus control; # $P < 0.05$ between indicated groups.

Abbreviations: ACP, amorphous calcium phosphate; *CAP*, cementum attachment protein; *CEMP1*, cementum protein I; COL, Type I collagen; *OCN*, osteocalcin; *OPN*, osteopontin; PCL, poly(ϵ -caprolactone); rhCEMP1, recombinant human cementum protein I; SD, standard deviation; Undet, undetected.

In vivo mineralized tissue regeneration

To investigate the osteoinductive and cementoinductive potential of the scaffolds, ACP/PCL/COL and rhCEMP1/ACP/PCL/COL were implanted orthotopically in the calvaria defect of a rat. None of the rats showed evidence of inflammatory or immune response after the implantation. All animals used in this experiment were sacrificed at 4 and 8 weeks.

Micro-CT images were examined to determine the degree of mineralization along with the distribution of the newly formed mineralized tissue. At 4 weeks, the control group (untreated defect; Figure 7A) remained open with minimal mineralized regions at the center of the defect or on regions confined mostly to the defect edges. For defects filled with ACP/PCL/COL scaffolds at 4 weeks, moderately mineralized regions with uniform bone growth were observed (Figure 7B). The edges of the regenerated calvarial defect appeared to be continuous with the surrounding bone in the control group, while bone regeneration was distributed through the ACP/PCL/COL scaffold surface layer by layer. The defects filled with rhCEMP1/ACP/PCL/COL had a much higher density (Figure 7C). At 8 weeks, defects in control and ACP/PCL/COL displayed almost complete closure (Figure 7D and E). However, the defects in rhCEMP1/ACP/PCL/COL remained open with some mineralized regions characterized by non-uniform low-density shadows (Figure 7F). The bone density of control and ACP/PCL/COL was quite similar at both 4 and 8 weeks. Mineralization took place, and bone density was doubled at 8 weeks. In contrast, the bone density in

rhCEMP1/ACP/PCL/COL was a little higher than the other groups at 4 weeks. However, it stopped increasing and ended up with a lower density at 8 weeks (Figure 7G).

Histological sections stained with H&E for calvaria defect treated with control, ACP/PCL/COL, and rhCEMP1/ACP/PCL/COL scaffolds at 4 and 8 weeks after the implantation of the scaffolds are shown in Figure 8. At 4 weeks, margins of the defect were connected by a thin connective fibrous tissue in the control, but no evidence of bone formation was observed (Figure 8A). For the defect treated with ACP/PCL/COL scaffold, it was almost filled with a layer of bonelike tissue (Figure 8B). Island-like new bone was distributed discretely in rhCEMP1/ACP/PCL/COL (Figure 8C). Further analysis at higher magnification using sections stained with H&E staining and Masson's trichrome staining exhibited abundant vascularization in ACP/PCL/COL (Figure 8H). A layer of regular cementum-like cells stained in purple was seen surrounding the rhCEMP1/ACP/PCL/COL. Adjacent to the targeted light purple cementum-like cells was a layer of ligament tissue. The outermost space was occupied by new bone (Figure 8I). The purple, light blue, and dark blue stained tissues constituted a sandwich structure resembling the periodontal complex. In Masson's trichrome staining, the sandwich structure was distinctly recognized, as the cementum-like layer was pink and purple, whereas the ligament layer and bone layer were light blue and dark blue, respectively (Figure 8O). At 8 weeks, similar tissue accumulated, except for new bone formation in the control

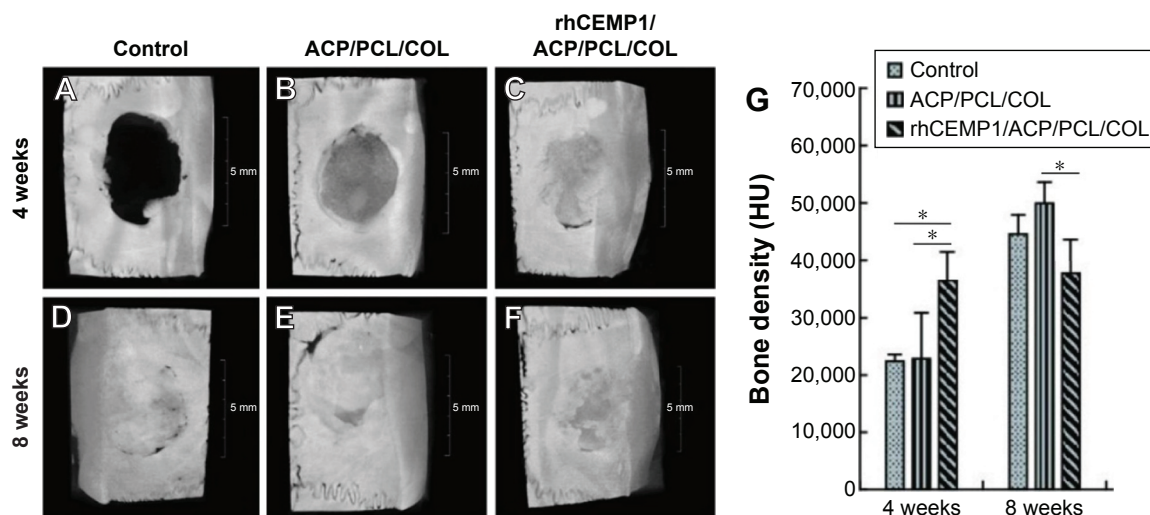


Figure 7 Evaluation of mineralization in calvarial defect via micro-CT showing mineralized bone formation at 4 and 8 weeks postimplantation of the scaffolds.

Notes: At 4 weeks, (A–C) the control group remained open while in ACP/PCL/COL and rhCEMP1/ACP/PCL/COL scaffolds moderately mineralized regions with uniform bone growth were observed. At 8 weeks, (D–E) defects in control and ACP/PCL/COL displayed almost complete closure. (F) The defects in rhCEMP1/ACP/PCL/COL remained open with some mineralized regions characterized by nonuniform low-density shadows. (G) The bone density in rhCEMP1/ACP/PCL/COL was a little higher than the other groups at 4 weeks. However, it ceased increasing and ended up with a lower density at 8 weeks. * $P < 0.05$.

Abbreviations: ACP, amorphous calcium phosphate; CEMP1, cementum protein 1; COL, type I collagen; CT, computed tomography; PCL, poly(ϵ -caprolactone); rhCEMP1, recombinant human cementum protein 1.

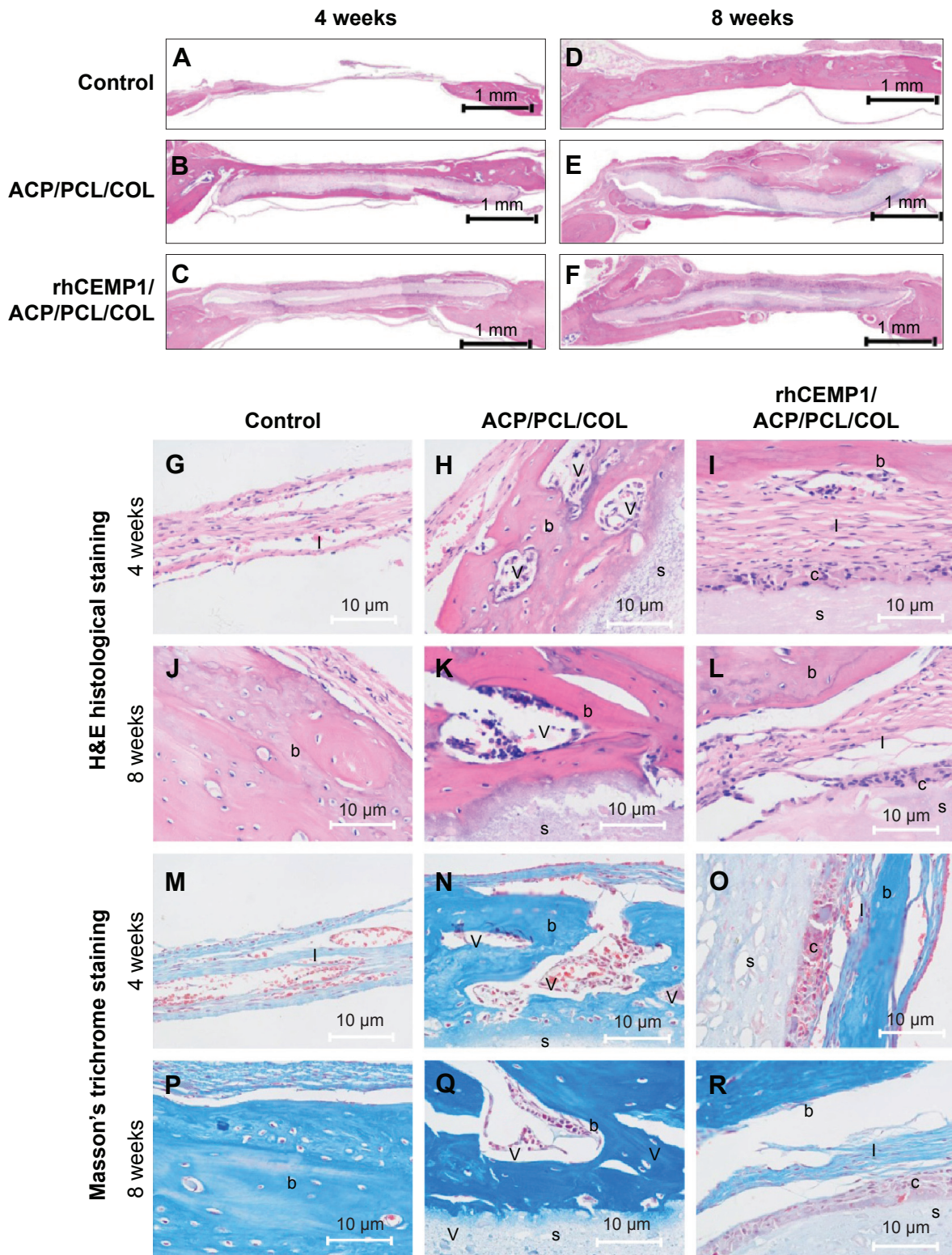


Figure 8 H&E histological staining and Masson's trichrome staining for samples from rat calvaria defect model after 4 and 8 weeks postimplantation.

Notes: (A and G) Control-4 weeks: margins of the defect are connected by a thin dense connective fibrous tissue; (B and H) ACP/PCL/COL-4 weeks: the defect is almost filled with bonelike tissue with vessels on the surface of the scaffold; (C) rhCEMP1/ACP/PCL/COL-4 weeks: there is not much new bone regenerating but a layer of regular cementum-like basophilic cells stained light blue-purple was seen surrounding the scaffold. Ligament-like tissue was seen adjacent to the bone-like tissue (I). (D and J) Control-8 weeks: the bonelike tissue formed showed lamellar features with limited small vessels. (E) ACP/PCL/COL-8 weeks: similar to (B) with more bone formation, abundant neovascularization was seen in (K). (F) rhCEMP1/ACP/PCL/COL-8 weeks: the defect has a closure of about 60% by bonelike tissue. Cementum-like tissue has an increment (L). Masson's trichrome staining (M-R). All microphotographs were taken at 400 \times magnification.

Abbreviations: ACP, amorphous calcium phosphate; b, bonelike tissue; c, cementum-like tissue; COL, type I collagen; H&E, hematoxylin and eosin; I, ligamentlike tissue; PCL, poly(ϵ -caprolactone); rhCEMP1, recombinant human cementum protein 1; s, scaffold; V, vessel.

(Figure 8D). Nonetheless, deficient vascularization hindered the extension of new bone (Figure 8J). Large amounts of bony nodules, both in number and size, were observed in ACP/PCL/COL, which led to the formation of the strips of bony tissue. These bony tissue islands were surrounded by dense connective tissue (Figure 8E, K, and Q). The layer of purple cementum-like tissue increased to more than 5-fold of the amount at 4 weeks. The bony island extended to 40%, leading to closure of the defect (Figure 8F). Masson's trichrome staining (Figure 8M–R) was similar to H&E (Figure 8G–L) staining, in which bonelike tissue, vessel, ligament-like tissue, cementum-like tissue were dark blue, red, light blue, and blue-purple, respectively.

Discussion

Considering the increasing aging population worldwide, there is a major need for the regeneration of periodontal tissue for maintaining normal tooth function. The ability to regenerate cementum tissue is crucial to this clinical challenge. We have designed and fabricated a novel multiphase scaffold with rhCEMP1, which can be released in a controlled manner. It was demonstrated that the rhCEMP1/ACP/PCL/COL scaffold has the potential of generating cementum-like tissue *in vitro* and *in vivo*. This may be a novel method to use a cementum-specific inductive scaffold for cementum regeneration, for which data has so far not been published.

In this study, it was observed that the rhCEMP1/ACP/PCL/COL scaffold enhanced the cementogenic differentiation of seeded PDLCs *in vitro* by upregulating the expression of typical cementoblastic gene markers CAP and CEMP1 while controlling the expression of osteoblastic gene markers OCN and OPN. Consequently, rhCEMP1/ACP/PCL/COL scaffold induced cementum-like tissue formation and hindered bone formation *in vivo* orthotopically compared to ACP/PCL/COL scaffold. These results demonstrate that the rhCEMP1 is a key bioactive compound in cementum formation both *in vitro* and *in vivo*.

Stem cells are one of the major players in tissue engineering approaches. The PDL tissue is a key contributor to the process of regeneration of the periodontium. It is quite complex and composed of several different cell populations, including osteoblasts and osteoclasts, cells of the epithelial rests of Malassez and cementoblasts. Besides, it also contains fibroblasts and undifferentiated mesenchymal stem cells.²⁹ CEMP1 can induce a cementoblastic phenotype and reduce osteoblastic differentiation in PDLCs.³⁰ A large animal model demonstrating *in situ* cementum regeneration must be further included in our study. PDL-derived cells would

have a more favorable effect on PDL formation instead of bone marrow mesenchymal stem cells.³¹ PDLCs served as stem cells in *in vitro* studies. However, the host provides the stem cell in *in vivo* experiments. The most appropriate *in vivo* model to evaluate the ability of CEMP1 to induce cementum regeneration would be the tooth root fenestration preclinical model.³² This model takes into consideration the functional loading of the tooth and should be regarded as an *in situ* cementum regeneration model. However, this model requires more sophisticated surgical techniques and longer time to treat samples. Therefore, we employed the critical size defect model as a preliminary assessment and this model could act as an ectopic cementum regeneration model. It is noteworthy that both bone and cementum are mineralized tissue, which have a higher density performance in micro-CT. CEMP1/ACP/PCL/COL exhibited the highest density at 4 weeks, as the micro-CT data showed. This high-density tissue manifested due to enhancement of mineralization and this mineralized tissue was proved to be cementum-like tissue in H&E sections.

This study shows that cementum regeneration is possible with a protein-releasing acellular biomaterial scaffold. In contrast to cell transplantation, this strategy of endogenous regeneration upon controlled releasing of rhCEMP1 offers a new approach to the reconstruction of periodontal complex. Despite the effective cementum induction, CEMP1 did not favor bone regeneration. However, Serrano et al³³ reported that rhCEMP1 was able to induce 97% regeneration of a rat calvaria critical-size defect, with the density and characteristics of the new mineralized tissues being normal for bone. This was probably because they applied rhCEMP1 to a gelatin matrix scaffold, which showed burst release. Moreover, gelatin was far more easily degraded, and so it was impossible to provide a sustained vehicle for rhCEMP1 in the 16-week experimental period.³⁴ Alizarin Red S staining showed PDLCs cultured in osteogenic induction medium increased mineralization, whereas CEMP1 overexpression completely inhibited the mineralization, which was in accordance with our study result.³⁰

Compared to the reparation of connective tissue and bone, the metabolism and reparation of cementum are much lower. That is probably why in clinical periodontitis treatment we would find that osteogenesis takes a dominant position, leading to ankylosed tooth and root absorption. Here in our study, rhCEMP1 slowed down the proliferation of stem cell growth, resulting in cementogenesis. Then, the expression of CAP, which symbolized cementogenesis, had increased to about 45 times as much as that of the control.

In vitro RT-PCR results showed that ACP/PCL/COL scaffold favored both osteogenic and cementogenic markers' expression. Particularly, ACP/PCL/COL upregulated the expression of CAP and CEMP1 (up to 2- and 20-fold). This seemed to be an inspiring sign. Nevertheless, we could hardly determine any cementogenesis apart from the new bone and vessels in in vivo experiment. The rhCEMP1/ACP/PCL/COL scaffold enhanced cementogenic differentiation of seeded PDLCs in vitro by upregulating the expression of typical cementoblastic gene markers CAP and CEMP1 while controlling the expression of osteoblastic gene markers OCN and OPN. It would be interesting to find out the possible molecular mechanism of how rhCEMP1 regulates cementogenesis. A microarray analysis aiming to assess differences in gene expression between cementoblasts and osteoblasts identified that the Wnt signaling pathway was differentially regulated. The expression of the Wnt inhibitors Wnt inhibitory factor 1 and secreted frizzled-related protein 1 was elevated in cementoblasts compared with osteoblasts.³⁵ Wnt signaling pathway is closely related to the regulation of cementogenesis.^{36,37} On the contrary, downregulation of Wnt causes root resorption.³⁸

Regarding the necessity of restoring cementum, periodontal ligament, and alveolar bone, which constitute the whole periodontal complex, a combination of more than one cytokine such as BMP2 for bone induction³⁹ and bFGF for periodontal ligament⁴⁰ is essential. However, more studies are needed to determine the most appropriate combination of double or triple cytokines. In addition, attention must be paid to the spatiotemporal delivery by modifying the delivery system on the basis of cell reaction in vitro.

Conclusion

In this study, we employed ACP as a sustainable delivery for rhCEMP1 in vivo. The release profile of the rhCEMP1/ACP nanoparticles was studied. Then, an electrospun multiphasic scaffold composed of rhCEMP1/ACP, PCL, and COL was fabricated and cocultured with PDLCs to assess the biocompatibility and inductivity. Finally, a critical size defect rat model was introduced to evaluate the effect of tissue regeneration of the scaffolds. The scaffold showed the ability to suppress cell proliferation behavior and upregulate the expression of cementoblastic markers while restricting the expression of osteoblastic markers when cocultured with human PDLCs in vitro for 7 days. Histology analysis after implantation in rats for 8 weeks showed that there was cementum-like tissue formation, but less bone formation. These results indicated the potential of using electrospun

multiphasic scaffolds for controlled release of rhCEMP1 for promoting cementum regeneration in reconstruction of the periodontal complex.

Acknowledgments

This study was supported by funds from National Natural Science Foundation of China (numbers: 51472115, 81271155, and 81300852), Jiangsu Province Natural Science Foundation of China (BK20130079), Key Project supported by Medical Science and Technology Development Foundation, Nanjing Department of Health (zqx13050), and Nanjing Scientific Development Project (201402035).

Disclosure

The authors report no conflicts of interest in this work.

References

1. Arzate H, Chimal-Monroy J, Hernández-Lagunas L, Díaz de León L. Human cementum protein extract promotes chondrogenesis and mineralization in mesenchymal cells. *J Periodontol Res*. 1996;31(2): 144–148.
2. Alvarez-Pérez MA, Pitaru S, Alvarez-Fregoso O, Reyes Gasga J, Arzate H. Anti-cementoblastoma-derived protein antibody partially inhibits mineralization on a cementoblastic cell line. *J Struct Biol*. 2003;143(1): 1–13.
3. Carmona-Rodríguez B, Alvarez-Pérez MA, Narayanan AS, et al. Human cementum protein 1 induces expression of bone and cementum proteins by human gingival fibroblasts. *Biochem Biophys Res Commun*. 2007;358(3):763–769.
4. Alvarez-Pérez MA, Narayanan S, Zeichner-David M, Rodríguez Carmona B, Arzate H. Molecular cloning, expression and immunolocalization of a novel human cementum-derived protein (CP-23). *Bone*. 2006;38(3):409–419.
5. Villarreal-Ramírez E, Moreno A, Mas-Oliva J, et al. Characterization of recombinant human cementum protein 1 (hrCEMP1): primary role in biomineralization. *Biochem Biophys Res Commun*. 2009;384(1): 49–54.
6. Zisch AH, Lutolf MP, Ehrbar M, et al. Cell-demanded release of VEGF from synthetic, biointeractive cell ingrowth matrices for vascularized tissue growth. *FASEB J*. 2003;17(15):2260–2262.
7. Lienemann PS, Lutolf MP, Ehrbar M. Biomimetic hydrogels for controlled biomolecule delivery to augment bone regeneration. *Adv Drug Deliv Rev*. 2012;64(12):1078–1089.
8. Ehrbar M, Djonov VG, Schnell C, et al. Cell-demanded liberation of VEGF121 from fibrin implants induces local and controlled blood vessel growth. *Circ Res*. 2004;94(8):1124–1132.
9. Jain RK. Normalization of tumor vasculature: an emerging concept in antiangiogenic therapy. *Science*. 2005;307(5706):58–62.
10. Rouwkema J, Rivron NC, van Blitterswijk CA. Vascularization in tissue engineering. *Trends Biotechnol*. 2008;26(8):434–441.
11. Park CH, Rios HF, Jin Q, et al. Biomimetic hybrid scaffolds for engineering human tooth-ligament interfaces. *Biomaterials*. 2010;31(23): 5945–5952.
12. Porter JR, Henson A, Popat KC. Biodegradable poly(epsilon-caprolactone) nanowires for bone tissue engineering applications. *Biomaterials*. 2009; 30(5):780–788.
13. Chastain SR, Kundu AK, Dhar S, Calvert JW, Putnam AJ. Adhesion of mesenchymal stem cells to polymer scaffolds occurs via distinct ECM ligands and controls their osteogenic differentiation. *J Biomed Mater Res A*. 2006;78(1):73–85.

14. Xin X, Hussain M, Mao JJ. Continuing differentiation of human mesenchymal stem cells and induced chondrogenic and osteogenic lineages in electrospun PLGA nanofiber scaffold. *Biomaterials*. 2007;28(2):316–325.
15. Shor L, Güçeri S, Wen X, Gandhi M, Sun W. Fabrication of three-dimensional polycaprolactone/hydroxyapatite tissue scaffolds and osteoblast-scaffold interactions in vitro. *Biomaterials*. 2007;28(35):5291–5297.
16. Ho SP, Senyrikova P, Marshall GW, et al. Structure, chemical composition and mechanical properties of coronal cementum in human deciduous molars. *Dent Mater*. 2009;25(10):1195–1204.
17. Stoecklin-Wasmer C, Rutjes AW, da Costa BR, Salvi GE, Jüni P, Sculean A. Absorbable collagen membranes for periodontal regeneration: a systematic review. *J Dent Res*. 2013;92(9):773–781.
18. Tadic D, Peters F, Epple M. Continuous synthesis of amorphous carbonated apatites. *Biomaterials*. 2002;23(12):2553–2559.
19. Zhang F, Allen AJ, Levine LE, et al. Structural and dynamical studies of acid-mediated conversion in amorphous-calcium-phosphate based dental composites. *Dent Mater*. 2014;30(10):1113–1125.
20. Yamamoto M, Hokugo A, Takahashi Y, Nakano T, Hiraoka M, Tabata Y. Combination of BMP-2-releasing gelatin/ β -TCP sponges with autologous bone marrow for bone regeneration of X-ray-irradiated rabbit ulnar defects. *Biomaterials*. 2015;56:18–25.
21. Chen X, Liu Y, Yang J, et al. The synthesis of hydroxyapatite with different crystallinities by controlling the concentration of recombinant CEMP1 for biological application. *Mater Sci Eng C Mater Biol Appl*. 2016;59:384–389.
22. Kuo YC, Ku IN. Cartilage regeneration by novel polyethylene oxide/chitin/chitosan scaffolds. *Biomacromolecules*. 2008;9(10):2662–2669.
23. Wu X, Miao L, Yao Y, et al. Electrospun fibrous scaffolds combined with nanoscale hydroxyapatite induce osteogenic differentiation of human periodontal ligament cells. *Int J Nanomedicine*. 2014;9:4135–4143.
24. Tanaka K, Iwasaki K, Feghali KE, Komaki M, Ishikawa I, Izumi Y. Comparison of characteristics of periodontal ligament cells obtained from outgrowth and enzyme-digested culture methods. *Arch Oral Biol*. 2011;56(4):380–388.
25. Spicer PP, Kretlow JD, Young S, Jansen JA, Kasper FK, Mikos AG. Evaluation of bone regeneration using the rat critical size calvarial defect. *Nat Protoc*. 2012;7(10):1918–1929.
26. Combes C, Rey C. Amorphous calcium phosphates: synthesis, properties and uses in biomaterials. *Acta Biomater*. 2010;6(9):3362–3378.
27. Li Y, Weng W, Cheng K, et al. Preparation of amorphous calcium phosphate in the presence of poly(ethylene glycol). *J Mater Sci Lett*. 2003;22:1015–1016.
28. Garzón A, Bravo I, Carrión-Jiménez MR, Rubio-Moraga Á, Albaladejo J. Spectroscopic study on binding of gentisic acid to bovine serum albumin. *Spectrochim Acta A Mol Biomol Spectrosc*. 2015;150:26–33.
29. Marchesan JT, Scanlon CS, Soehren S, Matsuo M, Kapila YL. Implications of cultured periodontal ligament cells for the clinical and experimental setting: a review. *Arch Oral Biol*. 2011;56(10):933–943.
30. Komaki M, Iwasaki K, Arzate H, Narayanan AS, Izumi Y, Morita I. Cementum protein 1 (CEMP1) induces a cementoblastic phenotype and reduces osteoblastic differentiation in periodontal ligament cells. *J Cell Physiol*. 2012;227(2):649–657.
31. Zhang J, Li ZG, Si YM, Chen B, Meng J. The difference on the osteogenic differentiation between periodontal ligament stem cells and bone marrow mesenchymal stem cells under inflammatory microenvironments. *Differentiation*. 2014;88(4–5):97–105.
32. Park CH, Rios HF, Jin Q, et al. Tissue engineering bone-ligament complexes using fiber-guiding scaffolds. *Biomaterials*. 2012;33(1):137–145.
33. Serrano J, Romo E, Bermúdez M, et al. Bone regeneration in rat cranium critical-size defects induced by Cementum Protein 1 (CEMP1). *PLoS One*. 2013;8(11):e78807.
34. Mathew P, Binulal NS, Nair SV, Selvamurugan N, Tamura H, Jayakumar R. Novel biodegradable chitosan–gelatin/nano-bioactive glass ceramic composite scaffolds for alveolar bone tissue engineering. *Chem Eng J*. 2010;158:353–361.
35. Matthews BG, Roguljic H, Franceschetti T, et al. Gene-expression analysis of cementoblasts and osteoblasts. *J Periodont Res*. Epub July 27, 2015.
36. Cao Z, Liu R, Zhang H, et al. Osterix controls cementoblast differentiation through downregulation of Wnt-signaling via enhancing DKK1 expression. *Int J Biol Sci*. 2015;11(3):335–344.
37. Shuqin L, Shan Y, Aishu R, Hongwei D. Investigation of Wnt/ β -catenin signaling pathway on regulation of Runx2 in cementoblasts under mechanical stress in vitro. *Hua Xi Kou Qiang Yi Xue Za Zhi*. 2015;33(1):35–39.
38. Lim WH, Liu B, Hunter DJ, Cheng D, Mah SJ, Helms JA. Downregulation of Wnt causes root resorption. *Am J Orthod Dentofacial Orthop*. 2014;146(3):337–345.
39. Sukul M, Nguyen TB, Min YK, Lee SY, Lee BT. Effect of local sustainable release of BMP2-VEGF from nano-cellulose loaded in sponge biphasic calcium phosphate on bone regeneration. *Tissue Eng Part A*. 2015;21(11–12):1822–1836.
40. Murakami S, Takayama S, Kitamura M, et al. Recombinant human basic fibroblast growth factor (bFGF) stimulates periodontal regeneration in class II furcation defects created in beagle dogs. *J Periodontal Res*. 2003;38(1):97–103.

International Journal of Nanomedicine

Publish your work in this journal

The International Journal of Nanomedicine is an international, peer-reviewed journal focusing on the application of nanotechnology in diagnostics, therapeutics, and drug delivery systems throughout the biomedical field. This journal is indexed on PubMed Central, MedLine, CAS, SciSearch®, Current Contents®/Clinical Medicine,

Submit your manuscript here: <http://www.dovepress.com/international-journal-of-nanomedicine-journal>

Dovepress

Journal Citation Reports/Science Edition, EMBASE, Scopus and the Elsevier Bibliographic databases. The manuscript management system is completely online and includes a very quick and fair peer-review system, which is all easy to use. Visit <http://www.dovepress.com/testimonials.php> to read real quotes from published authors.